Ultra-Compact Si-GST Hybrid Waveguides for Nonvolatile Light Wave Manipulation

Hanyu Zhang,[1] Linjie Zhou,[1*] B. M. A. Rahman,[2] Xing Wu,[3] Liangjun Lu,[1] Youhua Xu,[1] Jian Xu,[4] Junchao Song,[2] Zhigao Hu,[3], Liping Xu,[3] and Jianping Chen[1]

[1]Shanghai Institute for Advanced Communication and Data Science, State Key Laboratory of Advanced Optical Communication Systems and Networks, Department of Electronic Engineering, Shanghai Jiao Tong University, Shanghai 200240, China
[2]Department of Electrical and Electronic Engineering, City, University of London, Northampton Square, London EC 1V 0HB, U.K.
[3]Department of Electrical Engineering, East China Normal University, Shanghai, 200241, China
[4]Advanced Electronics Materials and Devices, Shanghai Jiao Tong University, Shanghai 200240, China

Abstract: Phase change materials (PCMs) combined with silicon photonics are emerging as a promising platform to realize miniature photonic devices. We study the basic optical properties of a sub-wavelength-dimension silicon ridge waveguide with a 20-nm-thick $Ge_2Sb_2Te_5$ (GST) top-clad layer. Numerical simulations show that the effective index of the Si-GST hybrid waveguide varies significantly when the GST changes from the amorphous to the crystalline states. This change can be utilized to make micron-size photonic devices. To experimentally verify the effectiveness of the Si-GST hybrid waveguide on light wave manipulation, we fabricated a series of unbalanced Mach-Zehnder interferometers with one arm connected with a section of Si-GST hybrid waveguide in different lengths. The transmission spectra are measured and the complex effective indices are extracted for GST at crystalline, amorphous and intermediate phases. The experimental results overall agree well with the simulation ones. The nonvolatile property of GST makes it attractive to reduce the static power consumption. This research represents a significant step towards the realization of ultra-compact Si-GST hybrid devices that will play a key role in high-density photonic integrated circuits, opening the door to many potential applications, including optical switch, memory and logic operation. Corresponding authors: Linjie Zhou (e-mail: ljzhou@sjtu.edu.cn)

Index Terms: Integrated Photonic Devices, Optical Switching Devices, Phase Change Material.

1. Introduction

Over the past decade, silicon has become an attractive device integration platform with the potential of large-scale integrations of both passive and active photonic components, together with the electronic drive circuits [1-3]. In order to build compact devices, resonant structures, such as ring resonators [4], disk resonators [5], Bragg gratings [6], and photonic crystals [7] are intensively investigated. However, due to their resonant feature, the optical bandwidth is sacrificed, limiting their employment in multiple applications. In addition, the resonant devices are very sensitive to temperature change owing to the relatively large thermo-optic coefficient of silicon, leading to practically unacceptable stability issues.

Phase change materials (PCMs) possess at least two reversible phases and have been considered as one of the most promising candidates to overcome some fundamental limitations in today's silicon photonic devices [8, 9]. The combination of PCMs with planar waveguides leads to ultrafast and ultra-compact optical devices [10]. In fact, the research of PCMs for optical applications began very early. The phase change was usually realized by laser irradiation. The first commercially successful application of PCMs was in rewritable optical data storage. At the same time, the scaling properties of the PCMs were studied [11-13]. It was found that the size effect starts to play an important role in the threshold field [14-16], the crystallization temperature [17-19], the crystallization speed [20, 21], and the work function [15]. The PCM transformation occurs in a time scale of nanosecond or even sub-nanosecond. The two stable and reversible states with distinguishable electrical, optical, and mechanical properties [22] make the PCM ideally suited for many potential optical applications, including display [23], optical signal processing [24], and optical switching [25-28]. In recent years, the scope for PCM has been extended to include oxides [8], such as vanadium dioxide. In this and other materials, the change in optical properties is enabled by temperature variation. However, the temperature-based phase change makes the devices volatile and need constant power to maintain one of its states [29].

The $Ge_2Sb_2Te_5$ (GST) is a well-known PCM material with its phase change occurred between crystalline (c-GST) and amorphous (a-GST) states. The phase change can be thermally [30], optically [26, 28, 31, 32] or electrically [33, 34] induced potentially with an ultra-high speed. Re-amorphorization is achieved by heating the crystalline phase above the melting point followed by rapid cooling. Crystallization is achieved by heating above the glass transition temperature and then slowly cooling down [35]. The GST possesses the "self-holding" feature [27], with no static power consumption required to maintain the states.

This paper presents theoretical and experimental study of ultra-compact Si-GST hybrid waveguides. It is organized as follows. First, the H-field based full vectoral finite-element method is used to find the field profile and the effective index of the hybrid waveguide mode. The least squares boundary residual (LSBR) method is used to find the transmission coefficients between the two discontinuous waveguide sections. Next, the device fabrication process flow and measurement are presented. Then, we characterize the Si-GST hybrid waveguide at the telecommunication wavelengths. The last part

gives the conclusions.

2. Theoretical Analysis

We obtain the refractive indices of a-GST and c-GST using the VASE ellipsometer. Figure 1 shows the extracted complex refractive index (n+ik) in dependence of wavelength. The increase of refractive index when GST transforms from the amorphous to the crystalline phase is due to a significant change in bonding [36]. Figure 2(a) shows the structure of a hybrid Si-GST waveguide. The silicon waveguide is a standard 500 nm (width) × 220 nm (height) single-mode waveguide with a slab layer thickness of 90 nm. A 20-nm-thick GST patch with a length of L_{GST} is placed on top of the silicon waveguide to form the hybrid waveguide. Figures 2(b) and 2(c) show the transverse and longitudinal cross sections of the hybrid waveguide.

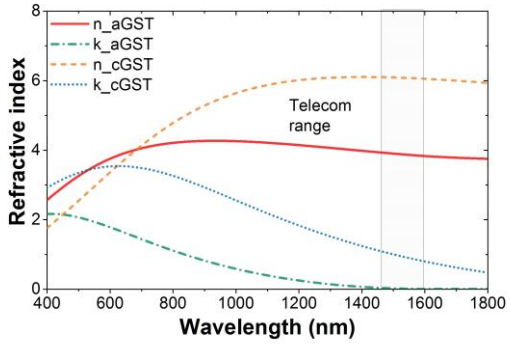

Fig. 1. Refractive index of GST as a function of wavelength. The GST is 20 nm thick on silicon substrate.

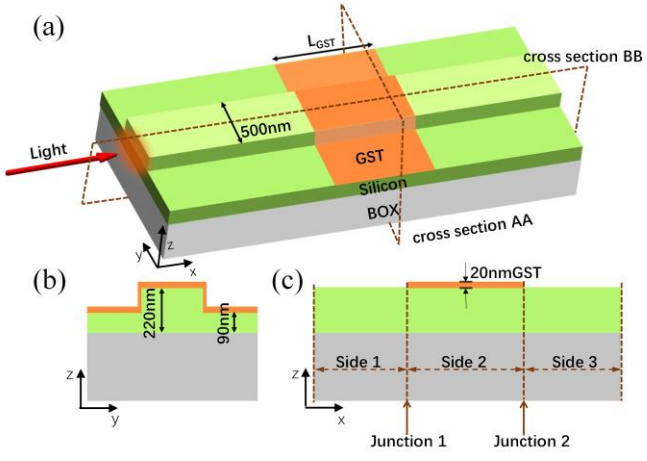

Fig. 2. (a) Schematic overview of the Si-GST hybrid waveguide. (b) Cross-sectional view along AA'. (c) Cross-sectional view along BB'.

We first study the property of the hybrid waveguide through numerical simulations. The operation wavelength is chosen at λ = 1.55 μm. The refractive indices of the materials at 1.55 μm are taken as n_{Si} = 3.481, n_{SiO2} = 1.445, $n_{a\text{-}GST}$ = 3.9027+0.0055i and $n_{c\text{-}GST}$ = 6.0769+0.9040i. The complex refractive index of GST is obtained from Fig. 1. We first use the H-field based full vectoral finite-element method (VFEM) to obtain the modal solutions of the waveguide. The VFEM has been established as one of the most accurate and numerically efficient approaches to obtain the modal field profiles and propagation constants of the fundamental and higher-order quasi-TE and quasi-TM modes. The full vectoral formulation is based on the minimization of the following energy function in terms of the nodal values of the full H-field vector [37]:

$$\omega^2 = \frac{\int (\nabla \times H)^* \cdot \varepsilon^{-1} \cdot (\nabla \times H) d\Omega + \rho (\nabla \cdot H)^* \cdot (\nabla \cdot H) d\Omega}{\int H^* \cdot \mu \cdot H d\Omega} \quad (1)$$

where H is the full vectoral magnetic field, * denotes the complex conjugate and transpose, ε and μ are the permittivity and permeability, respectively, ω^2 is the eigenvalue, where ω is the optical angular frequency of the wave, and ρ is a weighting factor for the penalty term.

When GST is in the amorphous phase, a low-loss quasi-TE polarized mode is supported and shown in Fig. 3(a), which is similar to the quasi-TE mode of a single-mode Si ridge waveguide. This quasi-TE mode has a calculated effective index of n_{eff} = 2.6328 and a propagation loss of 0.013 dB/μm. When GST is in the crystalline state, the waveguide supports a lossy mode as shown in Fig. 3(b). This lossy mode has a calculated effective index of n_{eff} = 2.8324 and a propagation loss of 4.038 dB/μm. Therefore, upon phase change of the GST material, the Si-GST hybrid waveguide can provide 4.025 dB/μm extinction ratio (ER), which is defined as the ratio between the maximum and the minimum output power transmissions.

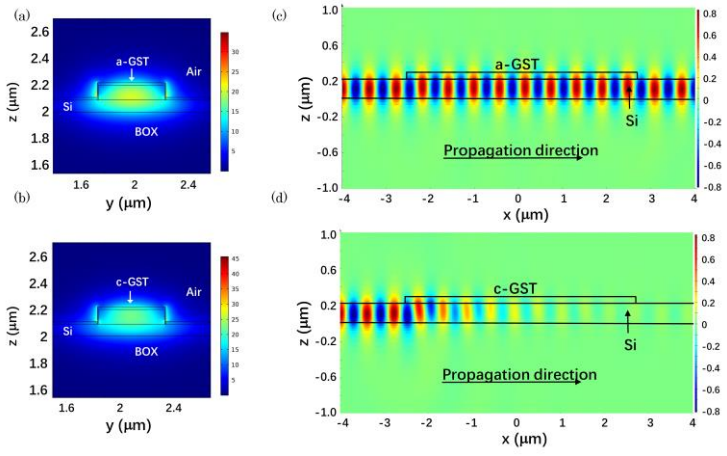

Fig. 3. (a, b) Calculated modal profiles of the Si-GST hybrid waveguide along the cross-section AA' when the GST is in (a) the amorphous state and (b) the crystalline state. (c, d) Electric field E_y component distribution along the propagation direction BB' when the GST is in (c) the amorphous state and (d) the crystalline state. The Si-GST hybrid waveguide length is 5 μm.

The power confinement factor, Γ_{mat}, measuring how well the optical power is confined in a certain material, is defined as [38]:

$$\Gamma_{mat} = \frac{\iint_{\Omega mat} E^* \times H dx dy}{\iint_{\Omega T} E^* \times H dx dy} \tag{2}$$

where the numerator integrates over the material region, Ω_{mat}, while the denominator integrates over the entire cross-section of the waveguide, Ω_T. Following this, Ω_{Si} of the hybrid waveguide is 74.4% and Ω_{GST} is 3.9% when GST is in the amorphous state; Ω_{Si} reduces to 69.7% and Ω_{GST} increases to 6% when GST is in the crystalline state. Besides, as the confinement in GST increases, the crystalline state has a larger propagation constant and a higher optical absorption loss.

The discontinuity between the regular silicon waveguide and the Si-GST hybrid waveguide introduces a waveguide junction, causing light scattering loss. The LSBR method has been applied on a wide range of discontinuity problems involving an abrupt change at the transverse plane. It can be used to achieve an accurate waveguide junction analysis and to obtain the power transfer. The LSBR method looks for a stationary solution to satisfy the continuity conditions for the tangential fields in a least squares sense by minimizing the error energy function J, which is defined as [39]:

$$J = \int \left| E_t^{\mathrm{I}} - E_t^{\mathrm{II}} \right|^2 + \alpha \cdot Z_0^2 \left| H_t^{\mathrm{I}} - H_t^{\mathrm{II}} \right|^2 d\Omega \tag{3}$$

Where E_t^I, H_t^{II} and E_t^{II}, H_t^{II} are the transverse electric and magnetic fields in the regular silicon waveguide and the Si-GST hybrid waveguide, respectively, Z_0 is the free-space impedance, and α is the dimensionless weighting factor to balance the electric and magnetic components of the error function J. The integration is carried out over the entire junction interface Ω. When GST is in the amorphous state, the total transmission loss through the two junctions is 0.09 dB for a 5-μm-long Si-GST hybrid waveguide. On the other hand, when GST is in the crystalline state, the total transmission loss increases to 20.5 dB.

To confirm the LSBR calculated results, we also perform the 3D finite-difference time-domain (FDTD) simulations. The fundamental quasi-TE mode of the silicon waveguide is launched into the input waveguide, and the transmitted power at the output end is monitored. Figures 3(c) and 3(d) show the electric field distributions along the waveguide longitudinal direction for the two states of GST, respectively. For the "on" state, where GST is in amorphous, the light can pass through the hybrid waveguide section with slight field attenuation. The transmission loss is 0.17 dB. However, for the "off" state, where GST is in crystalline, the field is rapidly attenuated when it goes into the hybrid waveguide section. The light is absorbed in the GST layer. The transmission loss is 24.1 dB. The FDTD results are overall consistent with the LSBR calculations.

3. Device Fabrication

To extract the effective index change of the Si-GST hybrid waveguide upon phase change, we designed an unbalanced Mach-Zehnder interferometer (MZI) structure as shown in Fig. 4(a). The MZI is composed of two 2 × 2 couplers connected by two waveguide arms with a length difference of ΔL = 400 μm. The Si-GST hybrid waveguide with a length L_{GST} is placed in the longer arm. We measured devices with various L_{GST} values from 0.3 μm to 7 μm. Figure 4(b) shows the optical microscope image of one typical device.

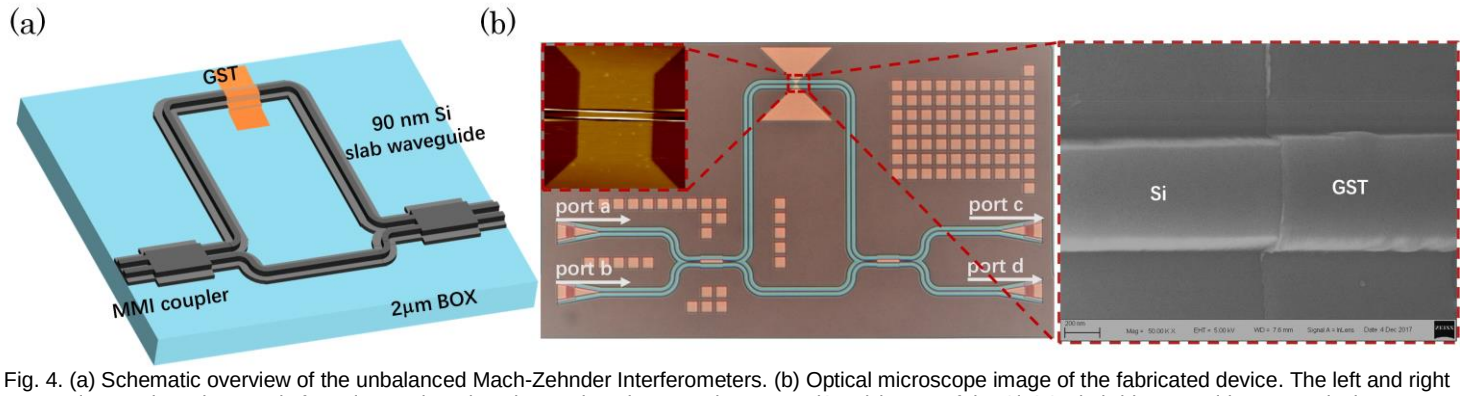

Fig. 4. (a) Schematic overview of the unbalanced Mach-Zehnder Interferometers. (b) Optical microscope image of the fabricated device. The left and right insets show the atomic force image (AFM) and scanning electron microscope (SEM) image of the Si-GST hybrid waveguide, respectively.

The devices were fabricated on a silicon-on-insulator wafer with a 220-nm thick top silicon layer and a 2-μm-thick buried oxide layer. The silicon waveguides were defined by 248 nm deep ultraviolet (DUV) photolithography and then etched by inductively coupled plasma (ICP) dry etch. Subsequently, poly-methyl-meth-acrylate (PMMA) resist was spin-coated and electron-beam lithography was used to define the GST window. A 20-nm-thick GST film was deposited using radio frequency (RF) sputtering from a stoichiometric $Ge_2Sb_2Te_5$ alloy target (20 W, 15 s.c.c.m. Argon gas, 0.0889 nm/min deposition rate). With RF sputtering, the composition of the deposited material was maintained. The GST was then patterned using lift-off process in a warm acetone bath.

So far, most research has focused on the switching properties of GST between a-GST and c-GST. However, during the phase transition, the GST film could also be at intermediate phases (i-GST) which incorporate combined portions of amorphous and crystalline phases. By controlling the degree of partial crystallization, the intermediate phase of GST can be produced, and thus a multi-level switchable optical property can be obtained for the GST film. The intermediate phase of the GST is dominated by both the annealing time and the annealing temperature [40].

The transmission spectrum of the devices was measured using a tunable laser scanning from 1520 nm to 1580 nm with a step size of 5 pm. A polarization controller was used to adjust the polarization to quasi-TE mode. Two single-mode fibers mounted at an angle of 10° were employed to couple light into and out of the device through on-chip grating couplers. The grating couplers were designed to be linearly chirped with an etched depth of 70 nm. The measured transmission spectra were all normalized to a reference straight waveguide to eliminate the influence of the grating couplers.

The waveguide effective index is determined not only by the refractive index of the waveguide material but also by the waveguide geometry and its surrounding. The evanescent interaction of the waveguide mode with the GST film results in a change in both the real and imaginary parts of the effective index. For each MZI, four transmission spectra from two input ports to two output ports were measured. The real part of the effective index change affects the phase of the arm, and thus the spectral shift. On the other hand, the imaginary part affects the loss of the arm, and thus the extinction ratio of the interference fringe in the spectrum. Therefore, by measuring the spectral shift and extinction ratio variation, we can extract the complex effective index change of the hybrid waveguide.

As a reference, the transmission spectra of MZIs without GST cladding were first tested. Next, the MZIs sputtering-coated with different lengths of GST patches were measured as state-1. Because the sputtering temperature is lower than the GST phase transition temperature, the as-deposited GST alloy is initially in the amorphous phase. In the state-2 and state-3, the devices were annealed for 4 min at 100 °C and 200 °C on a hot plate to reach i-GST, respectively. In the state-4, a 4-min annealing process at 245 °C on a hot plate was performed to obtain the c-GST. All samples were annealed in air.

4. Experimental Result and Discussion

Figure 5 shows the measured MZI spectra from input port-a to output port-c (see Fig. 4(b)) at different states. The Si-GST hybrid waveguide is 5 μm long. The interference fringe exhibits a high extinction ratio (>25 dB) when the GST is in the amorphous state, while it has a much lower extinction ratio (~5 dB) when GST changes to the crystalline state. This indicates that the c-GST has a much higher loss, leading to unbalanced optical power in the two arms. It is also observed that the fringe shifts after phase change, implying the real part of the effect index also varies.

To extract the effective index change, we use the transfer matrix method to model the MZI. The output fields E_c and E_d are related to the input fields E_a and E_b as:

$$\begin{bmatrix} E_c \\ E_d \end{bmatrix} = \begin{bmatrix} \tau_2 & j\kappa_2 \\ j\kappa_2 & \tau_2 \end{bmatrix} \cdot \begin{bmatrix} A\exp(j\phi) & 0 \\ 0 & 1 \end{bmatrix} \cdot \begin{bmatrix} \tau_1 & j\kappa_1 \\ j\kappa_1 & \tau_1 \end{bmatrix} \cdot \begin{bmatrix} E_a \\ E_b \end{bmatrix} \quad (4)$$

where τ_i and κ_i (i = 1, 2) are the field transmission and coupling coefficients of the couplers, respectively, A is the loss factor of the longer arm relative to the shorter one, and ϕ represents the phase difference between the MZI arms. We assume that the silicon waveguide loss is negligible compared to the Si-GST waveguide. The loss factor A is determined by the Si-GST waveguide and given by

$$A = \exp(-\frac{2\pi}{\lambda} \cdot k_{eff} \cdot L_{GST}) \tag{5}$$

where λ is the operation wavelength and k_{eff} is the imaginary part of the hybrid waveguide effective index. The phase difference ϕ is expressed as

$$\phi = \frac{2\pi}{\lambda}\left[n_{eff} \cdot L_{GST} + n_{neff,Si}\left(\Delta L - L_{GST}\right)\right] \tag{6}$$

where n_{eff} and $n_{eff,Si}$ are the effective indices of the hybrid silicon waveguide and regular silicon waveguide, respectively. The phase shift $\Delta\phi$ in the longer arm induces a spectral shift $\Delta\lambda = \Delta\phi \cdot FSR/2\pi$ with FSR being the free spectral range of the interference pattern. The real part of the effective index change $\Delta n_{eff,i}$ at state-i with respect to the reference (without GST) is given by

$$\Delta n_{eff,i} = \frac{\lambda}{FSR} \cdot \frac{\Delta\lambda_i}{L_{GST}} \qquad (i = 1,2,3,4) \tag{7}$$

where $\Delta\lambda_i$ is the spectral shift for state-i.

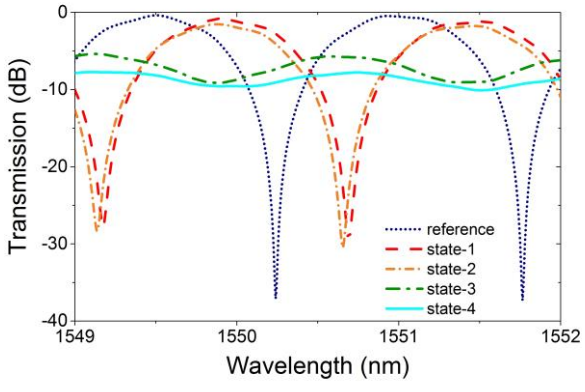

Fig. 5. Measured MZI transmission spectra when GST is at different states.

Figure 6(a) shows $\Delta\lambda_i$ as a function of L_{GST} obtained from the transmission spectrum measurement. As expected, $\Delta\lambda_i$ linearly increases with L_{GST}. The spectral shift $\Delta\lambda_2$ for state-2 is almost overlapped with $\Delta\lambda_1$ for state-1 (without annealing), suggesting that the 100°C annealing has a negligible effect on GST. From state-2 to state-4, the spectral shift increases with the annealing temperature. The maximum shift is achieved when the a-GST is fully converted to the c-GST at an annealing temperature of 245°C. It implies that the GST undergoes crystallization via an accumulated process. The i-GST was obtained at a moderate annealing temperature of 200°C in our experiment. In the intermediate states, small grains distribute uniformly over the observing area. The hexagonal-close-pack (HCP) phase co-exists with the face-center-cube (FCC) phase [41, 42]. By controlling the degree of partial crystallization, multi-level i-GST can be reached correspondingly. With linear fitting to the experimental spectral shift data and using (7), we can extract $\Delta n_{eff,i}$.

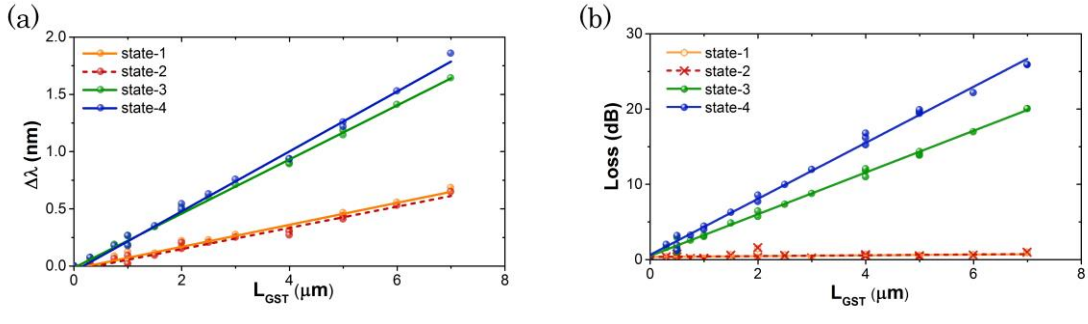

Fig. 6. (a) Spectral shift and (b) excess loss as a function of Si-GST hybrid waveguide length. The dots represent the experimental data and the straight lines are the linear fitting lines.

The loss factor A_i of the hybrid waveguide can be extracted by measuring the extinction ratios $R_{ac,i}$, $R_{ad,i}$, $R_{bc,i}$, and $R_{bd,i}$ of the four optical spectra, according to the following formula [43]:

$$A_i = \sqrt{\frac{\sqrt{R_{ad,i}} + (-1)^n \sqrt{R_{bc,i}} + (-1)^p}{\sqrt{R_{ad,i}} - (-1)^n \sqrt{R_{bc,i}} - (-1)^p}} = \sqrt{\frac{\sqrt{R_{ac,i}} + (-1)^l \sqrt{R_{bd,i}} + (-1)^m}{\sqrt{R_{ac,i}} - (-1)^l \sqrt{R_{bd,i}} - (-1)^m}} \quad (8)$$

where *m, n, l, p* are integers, taking 0 or 1. Following that, $k_{eff,i}$ can be obtained for the four states using Eq. (5). Figure 6(b) shows the excess loss, $-20 \cdot \log_{10}(A_i)$, of the hybrid waveguide as a function of L_{GST} when GST changes from state-1 to state-4.

Table 1 summarizes the extracted parameters for various GST states. The deposition of a-GST on the silicon waveguide causes its effective index to increase by 0.0924. After phase change to c-GST, the effective index increases by 0.259. The refractive index tuning range is thus 0.167, which is slightly smaller than the simulated value of 0.2. This presents an ultra-large refractive index tuning range compared to the thermo-optic or electro-optic effects in silicon. The propagation loss of the Si-GST hybrid waveguide is 0.05 dB/μm and 3.72 dB/μm for a-GST and c-GST, respectively. The simulation gives 0.013 dB/μm and 4.038 dB/μm propagation loss for the two states, slightly different from the experimental results.

Table 1 Extracted parameters of the Si-GST hybrid waveguide when the GST is at various states

State #	Annealing Condition	$\Delta\lambda_i/L_{GST}$ (nm/μm)	$\Delta n_{eff,i}$	$k_{eff,i}$	Loss (dB/μm)
1	no	0.0964	0.0924	0.004	0.05
2	100°C,4min	0.0932	0.0846	0.0041	0.05
3	200°C, 4min	0.237	0.244	0.083	2.77
4	245°C, 4min	0.263	0.259	0.113	3.72

The discrepancy can be caused by several factors. The GST film thickness is taken to be 20 nm in the simulation. However, in the real device, the thickness may deviate slightly. Figure 7 illustrates the impact of the GST film thickness variation on the hybrid waveguide effective index and propagation loss. It can be seen that when the thickness reduces by approximately 2 nm to 18 nm, both the effective index change and propagation loss at c-GST state have good agreement with the simulation. The measured higher loss at a-GST state is probably caused by the scattering loss due to the surface roughness of the GST layer. This scattering loss is likely overwhelmed by the material absorption loss in the c-GST state.

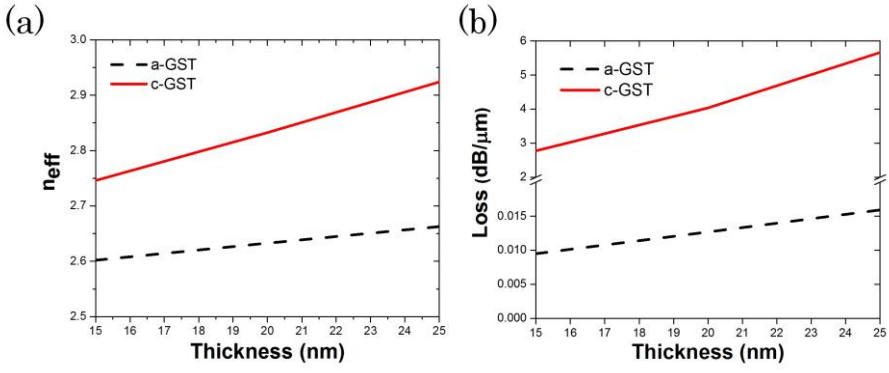

Fig. 7. VFEM simulation results showing the dependence of (a) the real part of the effective index and (b) and propagation loss of the Si-GST hybrid waveguide on the GST film thickness.

It has been shown that partial crystallization exists due to the accumulation process of the GST crystallization. As the degree of partial crystallization increases, the spectrum experiences gradual red shift with continuously reduced extinction ratio. Here, the crystallization and re-amorphization processes of the GST are enabled by thermal annealing. In fact, other stimulation methods can also be used, such as illumination by a laser with high peak power or using an electrical pulse. The typical switching time for electrical stimulation is in the order of nanoseconds. The silicon waveguide geometry used in our experiment also supports the quasi-TM mode with a high field amplitude at the top surface of the waveguide, which can potentially increases the interaction with the GST film [44]. The GST material itself has a higher loss (especially for c-GST) than silicon. However, in our hybrid waveguide design, a thin layer of GST only covers a very short length of silicon waveguide. It is enough to tune the effective index of the hybrid waveguide. For a 1-μm-long hybrid waveguide, the phase change of GST can lead to a considerable amount of spectral shift, and the excess loss at the a-GST state is only 0.05 dB, which is almost negligible. It can be employed to make 1x2 optical switches, for instance. It should be noted GST possess much lower loss in the longer wavelength band from 1800 nm to 2100 nm [45]. The hybrid waveguide propagation loss can be reduced considerably in this wavelength band. The GST material that we used is just one type of candidate phase-change material. In fact, there exist a great variety of other phase-change materials, such as GeSe [27], $Ge_2Sb_2Se_4Te_1$ [46], etc. They have lower loss at the 1550 nm wavelength, which are worth further exploration in the future work.

5. Conclusions

We have investigated a Si-GST hybrid waveguide that can be used for nonvolatile light wave manipulation. The hybrid waveguide experiences a large refractive effective index modulation upon phase change of the GST material. Using an unbalanced MZI structure with one arm connected with a Si-GST hybrid waveguide, we extracted the complex refractive index changes at various GST phase states. The real part effective index change from a-GST to c-GST is 0.167. The propagation loss of the Si-GST hybrid waveguide for a-GST and c-GST is 0.05 dB/ μm and 3.72 dB/ μm, respectively. The experimental results overall agree with the simulation prediction. The crystallization level can be well controlled by adjusting the annealing conditions, resulting in intermediate GST phases. The GST possesses the “self-holding” feature, making it very attractive for low power applications. The Si-GST hybrid waveguide can be used to construct micrometer-sized photonic devices, paving the way for realization of ultra-compact photonic integrated circuits.

Acknowledgements

This work was supported in part by the National Natural Science Foundation of China (NSFC) (61661130155, 61422508). We also would like to thank Dr. Richard A. Soref for the insightful discussion.

References

[1] P. Dong, Y.-K. Chen, G.-H. Duan, and D. T. Neilson, "Silicon photonic devices and integrated circuits," *Nanophotonics,* vol. 3, no. 4-5, 2014.

[2] H. Subbaraman *et al.*, "Recent advances in silicon-based passive and active optical interconnects," *Opt Express,* vol. 23, no. 3, pp. 2487-510, Feb 09 2015.

[3] D. Thomson *et al.*, "Roadmap on silicon photonics," *Journal of Optics,* vol. 18, no. 7, p. 073003, 2016.

[4] Y. Hu *et al.*, "High-speed silicon modulator based on cascaded microring resonators," *Opt Express,* vol. 20, no. 14, pp. 15079-85, Jul 02 2012.

[5] H. Chen and A. W. Poon, "Two-photon absorption photocurrent in p-i-n diode embedded silicon microdisk resonators," *Appl Phys Lett,* vol. 96, no. 19, p. 191106, 2010.

[6] Z. Zou, L. Zhou, X. Li, and J. Chen, "60-nm-thick basic photonic components and Bragg gratings on the silicon-on-insulator platform," *Opt Express,* vol. 23, no. 16, pp. 20784-95, Aug 10 2015.

[7] Y. Jiang, W. Jiang, L. Gu, X. Chen, and R. T. Chen, "80-micron interaction length silicon photonic crystal waveguide modulator," *Appl Phys Lett,* vol. 87, no. 22, p. 221105, 2005.

[8] M. Wuttig, H. Bhaskaran, and T. Taubner, "Phase-change materials for non-volatile photonic applications," *Nature Photonics,* vol. 11, no. 8, pp. 465-476, 2017.

[9] T. Moriyama *et al.*, "Ultra-compact, self-holding asymmetric Mach-Zehnder interferometer switch using $Ge_2Sb_2Te_5$ phase-change material," *IEICE Electronics Express,* vol. 11, no. 15, pp. 20140538-20140538, 2014.

[10] C. Ríos *et al.*, "Integrated all-photonic non-volatile multi-level memory," *Nature Photonics,* vol. 9, no. 11, pp. 725-732, 2015.

[11] X. Sun, B. Yu, and M. Meyyappan, "Synthesis and nanoscale thermal encoding of phase-change nanowires," *Appl Phys Lett,* vol. 90, no. 18, p. 183116, 2007.

[12] Y. Jung, S. H. Lee, D. K. Ko, and R. Agarwal, "Synthesis and characterization of $Ge_2Sb_2Te_5$ nanowires with memory switching effect," *J Am Chem Soc,* vol. 128, no. 43, pp. 14026-7, Nov 01 2006.

[13] S. H. Lee, Y. Jung, and R. Agarwal, "Highly scalable non-volatile and ultra-low-power phase-change nanowire memory," *Nat Nanotechnol,* vol. 2, no. 10, pp. 626-30, Oct 2007.

[14] D. Krebs, S. Raoux, C. T. Rettner, G. W. Burr, M. Salinga, and M. Wuttig, "Threshold field of phase change memory materials measured using phase change bridge devices," *Appl Phys Lett,* vol. 95, no. 8, p. 082101, 2009.

[15] H. Tong, Z. Yang, N. N. Yu, L. J. Zhou, and X. S. Miao, "Work function contrast and energy band modulation between amorphous and crystalline $Ge_2Sb_2Te_5$ films," *Appl Phys Lett,* vol. 107, no. 8, p. 082101, 2015.

[16] Y. C. Chen *et al.*, "Ultra-thin phase-change bridge memory device using GeSb," (in English), *International electron devices meeting international conference,* San Francisco, USA, 2006, pp. 531-534.

[17] J. W. Galusha, L. R. Richey, M. R. Jorgensen, J. S. Gardner, and M. H. Bartl, "Study of natural photonic crystals in beetle scales and their conversion into inorganic structures via a sol–gel bio-templating route," *J. Mater. Chem.,* vol. 20, no. 7, pp. 1277-1284, 2010.

[18] H. F. Hamann, M. O'Boyle, Y. C. Martin, M. Rooks, and H. K. Wickramasinghe, "Ultra-high-density phase-change storage and memory," *Nat Mater,* vol. 5, no. 5, pp. 383-7, May 2006.

[19] H. Satoh, K. Sugawara, and K. Tanaka, "Nanoscale phase changes in crystalline $Ge_2Sb_2Te_5$ films using scanning probe microscopes," *J Appl Phys,* vol. 99, no. 2, p. 024306, 2006.

[20] S. Raoux *et al.*, "Phase-change random access memory: A scalable technology," *IBM J Res Dev,* vol. 52, no. 4.5, pp. 465-479, 2008.

[21] G. W. Burr *et al.*, "Phase change memory technology," *Journal of Vacuum Science & Technology B, Nanotechnology and Microelectronics: Materials, Processing, Measurement, and Phenomena,* vol. 28, no. 2, pp. 223-262, 2010.

[22] S. Raoux, F. Xiong, M. Wuttig, and E. Pop, "Phase change materials and phase change memory," *MRS Bulletin,* vol. 39, no. 08, pp. 703-710, 2014.

[23] P. Hosseini, C. D. Wright, and H. Bhaskaran, "An optoelectronic framework enabled by low-dimensional phase-change films," *Nature,* vol. 511, no. 7508, pp. 206-11, Jul 10 2014.

[24] L. Zou, M. Cryan, and M. Klemm, "Phase change material based tunable reflectarray for free-space optical inter/intra chip interconnects," *Opt Express,* vol. 22, no. 20, pp. 24142-8, Oct 06 2014.

[25] Y. Hu *et al.*, "Nanosecond switching in superlattice-like GeTe/Sb thin film for high speed and low power phase change memory application," *ECS Journal of Solid State Science and Technology,* vol. 6, no. 1, pp. P45-P48, 2016.

[26] M. Rudé *et al.*, "Optical switching at 1.55 μm in silicon racetrack resonators using phase change materials," *Appl Phys Lett,* vol. 103, no. 14, p. 141119, 2013.

[27] R. Soref, "Phase-change materials for Group-IV electro-optical switching and modulation," *12th International Conference on Group IV Photonics,* Vancouver, Canada, 2015, pp. 157-158.

[28] D. Tanaka *et al.*, "Ultra-small, self-holding, optical gate switch using $Ge_2Sb_2Te_5$ with a multi-mode Si waveguide," *Opt Express,* vol. 20, no. 9, pp. 10283-94, Apr 23 2012.

[29] A. Joushaghani, J. Jeong, S. Paradis, D. Alain, J. Stewart Aitchison, and J. K. Poon, "Wavelength-size hybrid Si-VO_2 waveguide electroabsorption optical switches and photodetectors," *Opt Express,* vol. 23, no. 3, pp. 3657-68, Feb 9 2015.

[30] M. Stegmaier, C. Ríos, H. Bhaskaran, and W. H. P. Pernice, "Thermo-optical effect in phase-change nanophotonics," *ACS Photonics,* vol. 3, no. 5, pp. 828-835, 2016.

[31] T. Moriyama, H. Kawashima, M. Kuwahara, X. Wang, H. Asakura, and H. Tsuda, "Small-sized Mach-Zehnder interferometer optical switch using thin film $Ge_2Sb_2Te_5$ phase-change material," *Optical Fiber Communications Conference and Exhibition,* San Francisco, USA, 2014, p. Tu3E.4.

[32] Y. Ikuma *et al.*, "Reversible optical gate switching in Si wire waveguide integrated with $Ge_2Sb_2Te_5$ thin film," *Electron Lett,* vol. 46, no. 21, p. 1460, 2010.

[33] K. Kato, M. Kuwahara, H. Kawashima, T. Tsuruoka, and H. Tsuda, "Current-driven phase-change optical gate switch using indium–tin-oxide heater," *Applied Physics Express,* vol. 10, no. 7, p. 072201, 2017.

[34] F. Xiong, A. D. Liao, D. Estrada, and E. Pop, "Low-power switching of phase-change materials with carbon nanotube electrodes," *Science,* vol. 332, no. 6029, pp. 568-70, Apr 29 2011.

[35] R. L. Cotton and J. Siegel, "Stimulated crystallization of melt-quenched $Ge_2Sb_2Te_5$ films employing femtosecond laser double pulses," *J Appl Phys,* vol. 112, no. 12, p. 123520, 2012.

[36] K. Shportko, S. Kremers, M. Woda, D. Lencer, J. Robertson, and M. Wuttig, "Resonant bonding in crystalline phase-change materials," *Nat Mater,* vol. 7, no. 8, pp. 653-8, Aug 2008.

[37] B. M. A. Rahman and J. B. Davies, "Finite-element solution of integrated optical waveguides," *J Lightwave Technol,* vol. 2, no. 5, pp. 682-688, 1984.

[38] B. M. A. Rahman and J. B. Davies, "Finite Element Modelling Methods for Photonics " *Massachusetts Artech House,* Boston, 2013, Chap. 2.

[39] B. M. A. Rahman and J. B. Davies, "Analysis of optical waveguide discontinuities," *J Lightwave Technol,* vol. 6, no. 1, pp. 52-57, 1988.

[40] K.-K. Du *et al.*, "Control over emissivity of zero-static-power thermal emitters based on phase-changing material GST," *Light: Science & Applications,* vol. 6, no. 1, p. e16194, 2016.

[41] L. Zhang, X. Han, and Z. Zhang, "Crystallization process of in situ annealed $Ge_2Sb_2Te_5$ films," *Journal of Alloys and Compounds,* vol. 537, pp. 71-75, 2012.

[42] Y. Wu, K. Liu, D. Li, Y. Guo, and S. Pan, "In situ AFM and Raman spectroscopy study of the crystallization behavior of $Ge_2Sb_2Te_5$ films at different temperature," *Applied Surface Science,* vol. 258, no. 4, pp. 1619-1623, 2011.

[43] M. A. Tran, T. Komljenovic, J. C. Hulme, M. L. Davenport, and J. E. Bowers, "A Robust Method for Characterization of Optical Waveguides and Couplers," *IEEE Photonics Technology Letters,* vol. 28, no. 14, pp. 1517-1520, 2016.

[44] N. Gruhler, C. Benz, H. Jang, J. H. Ahn, R. Danneau, and W. H. Pernice, "High-quality Si_3N_4 circuits as a platform for graphene-based nanophotonic devices," *Opt Express,* vol. 21, no. 25, pp. 31678-89, Dec 16 2013.

[45] H. Liang, R. Soref, J. Mu, A. Majumdar, X. Li, and W.-P. Huang, "Simulations of Silicon-on-Insulator channel-waveguide electrooptical 2 × 2 switches and 1 × 1 modulators using a $Ge_2Sb_2Te_5$ self-holding Layer," *J Lightwave Technol,* vol. 33, no. 9, pp. 1805-1813, 2015.

[46] Y. Zhang et al., "Broadband transparent optical phase change materials," Conference on Lasers and Electro-Optics, San Jose, California United States, 2017, paper JTh5C.4.